Article

Modeling Silicon-Dominant Anodes: Parametrization, Discussion, and Validation of a Newman-Type Model

Axel Durdel [1,*], Sven Friedrich [1], Lukas Hüsken [1], and Andreas Jossen [1]

Chair of Electrical Energy Storage Technology, Department of Energy and Process Engineering, School of Engineering and Design, Technical University of Munich, Arcisstraße 21, 80333 Munich, Germany
* Correspondence: axel.durdel@tum.de

S1. Supplementary Information on Electrode Composition and Morphology

Anode Composition

The silicon (Si) anode active material consists of micrometer Si particles (CLM00001, Wacker Chemie AG, Germany). The anode composite in turn consists of 69.70 wt% Si, 19.90 wt% graphite (Gr conductive agent) (C-NERGY^{TM} KS6L, Imerys Graphite & Carbon Ltd., Switzerland), 2.00 wt% CB (carbon black) (C-NERGY Super C65, Imerys Graphite & Carbon Ltd., Switzerland), 8.20 wt% lithium polyacrylate (LiPAA binder) (Sigma-Aldrich Chemie GmbH, Germany), and 0.20 wt% carboxymethyl cellulose (CMC binder) (CMC MAC200HC, Nippon Paper Industries Co., Ltd., Japan). The graphite is electrochemically inactive and only serves as a conductive agent [1]. The composite is coated on a 12 µm copper foil (SE-Cu, Schlenk Metallfolien GmbH & Co. KG, Germany). An overview on the coating composition is given in Table S1.

Cathode Composition

The cathode active material consists of nickel-cobalt-aluminum-oxide (NCA) in a molar composition of $LiNi_{0.8}Co_{0.15}Al_{0.05}O_{1.985}(BO_3)_{0.01}$ (fractions given in mol%, HED^{TM} NCA-7051-b, BASF SE, Germany). The cathode composite in turn consists of 96.00 wt% NCA, 2.00 wt% carbon black and 2.00 wt% polyvinylidene difluoride (PVdF binder) (Solef 5130, Solvay, Belgium). The composite is coated on a 15 µm aluminum foil (1100-L Hydro series, Norsk Hydro ASA, Norway). An overview on the coating composition is given in Table S1.

Separator Properties

The separator used in the coin cells and in the T-cells is a glass fiber separator (type 691, VWR International GmbH, Germany) with a thickness of 260 µm each. A porosity of 93% is calculated from measurements of the sample mass and volume in the uncompressed state.

Coating Geometry and Morphology

The coating thicknesses including the current collector foil are measured at several points along the electrode sheet using a micrometer measuring screw (accuracy ±1 µm, Micromahr IP40, Carl Mahr Holding GmbH, Germany), which directly gives the (average) thickness of a single sample (see Table S1).

The porosities ε_l and active material volume fractions ε_{AM} of the electrode coatings are calculated based on the composition of the respective coating composite and measured masses and thicknesses. All necessary data are given in Tables S1 and S2. The resulting values are given in Table B.2 in the main document. Since the thickness and mass of the electrode samples were measured after calendering and before cell assembly, and as

such before cell formation, the given values are pristine values prior to the amorphization process of the Si electrodes.

$$\varepsilon_1 = 1 - \frac{V_\text{s}}{V_\text{coat}} = 1 - \frac{\sum_i \frac{m_{\text{rel},i}}{\rho_i} \cdot m_\text{coat}}{A \cdot (L_\text{tot} - L_\text{CC})} \tag{S1}$$

$$\varepsilon_\text{AM} = \frac{V_\text{AM}}{V_\text{coat}} = \frac{\frac{m_{\text{rel,AM}}}{\rho_\text{AM}} \cdot m_\text{coat}}{A \cdot (L_\text{tot} - L_\text{CC})} \tag{S2}$$

Here, V_s is the volume of all solid phase components of a representative volume element (RVE) with a total coating volume of V_coat, $m_{\text{rel},i}$ is the weight-percentage of the component i, ρ_i is its density, and m_coat is the total weight of the coating. Considering a sample area of A, the total weight of a coated electrode sample and that of the current collector (CC) without a coating can be measured individually and give the total weight of the coating. The total volume of the the the coating V_coat, i.e., the RVE, is based on the sample area A and the difference between the measured thicknesses of the sample with coating L_tot and that of an uncoated current collector L_CC. For the calculation of the active material volume fraction, $m_{\text{rel,AM}}$ is the weight-percentage of the active material phase and ρ_AM is its density. The corresponding values for a $\varnothing 15$ mm sample are given in Tables S1 and S2, and the results are listed in Table B.2 in the main document.

The MacMullin numbers for the anode and cathode composites are calculated based on tortuosity measurements using symmetrical cells. The MacMullin number is calculated according to Equation S3. Here, the tortuosity τ is measured using symmetrical cells as described by Landesfeind et al. [2] and ε_1 is the porosity as described above.

$$N_\text{M} = \frac{\tau}{\varepsilon_1} \tag{S3}$$

The resulting MacMulling numbers are 5.385 and 7.333 for the anode and cathode, respectively. For the glass fiber separator, Habedank et al. [3] assumed a tortuosity of 1.2. This yields a MacMullin number of 1.29. The values are summarized in Table B.2 in the main document.

Table S1. Electrode composition including mass densities for each component as needed for Equations S1 and S2.

Component	Anode m_rel in wt%	Cathode m_rel in wt%	Density ρ in g cm^{-3}
Si	69.70	—	2.336
Gr	19.90	—	2.26
LiPAA	8.20	—	1.2
CMC	0.2	—	1.6
CB	2.00	2.00	2.00
NCA	—	96.00	4.73
PVdF	—	2.00	1.76

S2. Supplementary Information on Cell Assembly

In this work, circular coin cells (CR2032) for characterization as well as Swagelok® T-cells for validation are used. All cells were assembled in an argon-filled glove-box (H_2O and $O_2 < 0.1$ ppm, M. Braun Intergas-Systeme GmbH, Germany). The electrode samples used here were punched out of the coated electrode sheet ($\varnothing 14.00$ mm for coin cells, $\varnothing 10.95$ mm for T-cells). The electrolyte in all cells is 1M LiPF$_6$ in FEC:DEC (1:4 by vol., Gotion, USA).

Using the coin cell setup, only a two-electrode system is possible. Accordingly, different coin cells were assembled, one anode half cell vs. lithium (Li) metal, one cathode half cell vs. Li metal, and one NCA∣∣Si full cell. The interior of the coin half cells consists

Table S2. Characteristic properties of double-coated electrode samples as needed for Equations S1 and S2. Thickness values of the coated electrodes were measured after electrode calendering and prior to cell assembly and formation. Values for the current collector (CC) were measured using uncoated foils.

	Symbol	Unit	Anode	Cathode
Sample diameter		mm	15.00	15.00
Total weight	m_{tot}	mg	37.10	79.64
CC weight	m_{CC}	mg	19.76	7.35
Total thickness	L_{tot}	µm	104	151
CC thickness	L_{CC}	µm	12	15

of one 500 µm aluminum spacer, one 250 µm Li foil (⌀15.60 mm), two 260 µm glass fiber separators (⌀16.00 mm, type 691, VWR) filled with 90 µL electrolyte, an electrode sample (⌀14.00 mm, coated on one side only, for thickness see Table B.2 in the main document), one 1000 µm aluminum spacer, and one disc spring. The interior of the coin full cells is similar to that of the half cells, but the Li foil is replaced by the anode sample (⌀15.60 mm) and the 500 µm spacer is replaced by a 1000 µm spacer in order to provide a similar mechanical pressure due to the thickness difference between the Li metal and the counter electrode. The setup results in a stack pressure of approximately 0.2 MPa. The cells rested for six hours after assembly for the wetting process to be complete.

The Swagelok® T-cell with its three-electrode setup allows for simultaneous measurement of the half cell and full cell potentials. The full cell stack consists of a negative electrode sample (⌀10.95 mm), two 260 µm glass fiber separators (⌀10.95 mm, type 691, VWR), and one positive electrode sample (⌀10.95 mm, coated on one side only). The thickness values of the anode and cathode coatings are given in Table B.2 in the main document. The separator closer to the anode has a small flap that serves as an ionic pathway to the reference electrode. The reference electrode is an Li metal chip and is ionically connected to the electrolyte via this flap and another separator of the same type (⌀10.00 mm). The separators between the working and counter electrodes are filled with 60 µL electrolyte and the single separator on the reference side is filled with additional 40 µL electrolyte. The full cell stack is spring-compressed to approximately 0.2 MPa.

During cell assembly, the weight of the coated electrode (current collector and coating) as well as the weight of the pure current collector of the same size were measured, which give the mass of the coating. Considering the active material volume fraction given in Table B.2 in the main document, this also gives the mass of active material. The nominal capacity of the cell is given by the gravimetric capacity of the limiting electrode and its total active material mass. For the cell setup in this work, the gravimetric capacity of NCA is defined as 185 mAh g_{NCA}^{-1} on full cell level. For Si in this work, however, the gravimetric capacity is defined as 1200 mAh g_{Si}^{-1}, which corresponds to a partial lithiation of silicon of approximately 33.5% considering 3579 mAh g^{-1} for full lithiation to $Li_{15}Si_4$ [4]. The concept of partial lithiation is based on the findings of Jantke et al. [1]. The nominal capacities C_N are 5.809 mAh for the NCA cathode coin half cell and the coin full cell, and 6.636 mAh for the Si anode coin half cell. The nominal capacity for the T-cell is 3.110 mAh.

S3. Supplementary Information on Operational Procedures

Cell Formation and Stabilization

After cell assembly, the cells underwent a formation and stabilization procedure (see Table S3). All tests were carried out at 25 °C. The coin cells have been operated in a KT 170 climate chamber (Binder, Germany) and cycled using a BaSyTec CTS (BaSyTec, Germany). Note that the cell temperature is assumed to be constant for all tests because the total heat capacity of the cell setup including the housing is expected to buffer all cell heating. The T-cells were operated in a custom-built climate chamber and cycled using a BioLogic VMP3

potentiostat (BioLogic SAS, France). The NCA coin half cell was cycled between 3.0 V and 4.4 V for all tests and the coin full cell as well as the T-cell were cycled between 2.8 V and 4.2 V.

Table S3. Cycling procedure for the formation (cycle 1), the stabilization (cycle 2–10), and the quasi open-circuit potential measurement (cycle 11–13) for the coin and T-cell full cells (FC) as well as the NCA and Si coin half cells (HC). In this table the nomenclature for the "charge" and "discharge" steps is that of a full cell, i.e., Si on the anode side and NCA on the cathode side. Hence, the charge step is equal to a lithiation of the Si anode and a delithiation of the NCA cathode and vice versa for the discharge step.

Cycle	Charge				Discharge			
		Termination				Termination		
		FC	NCA HC	Si HC		FC	NCA HC	Si HC
1	CC $I = $ C/15	$U > 4.2$ V	$U > 4.4$ V	$C > C_N$ [1]	CC $I = $ C/15	$U < 2.8$ V	$U < 3.0$ V	$U > 1.0$ V
2–3	CC $I = $ C/10	$U > 4.2$ V	$U > 4.4$ V	$C > C_{rev}$ [2]	CC $I = $ C/10	$U < 2.8$ V	$U < 3.0$ V	$U > 1.0$ V
4–6	CC $I = $ C/10 CV[3] $U = 4.2$ V	$U > 4.2$ V $I < $ C/20	$U > 4.4$ V $I < $ C/20	$C > C_{rev}$ [2]	CC $I = $ C/10	$U < 2.8$ V	$U < 3.0$ V	$U > 1.0$ V
7–10	CC $I = $ C/2 CV[3] 4.2 V	$U > 4.2$ V $I < $ C/20	$U > 4.4$ V $I < $ C/20	$C > C_{rev}$ [2]	CC $I = $ C/2	$U < 2.8$ V	$U < 3.0$ V	$U > 1.0$ V
11–13	CC $I = $ C/50 CV[4] 4.2 V	$U > 4.2$ V $I < $ C/200	$U > 4.4$ V	$U < 0.170$ V	CC $I = $ C/50 CV[4] 2.8 V	$U < 2.8$ V $I < $ C/200	$U < 3.0$ V	$U > 1.0$ V

[1] C_N: nominal capacity based on active material mass and self-defined gravimetric capacity of 185 mAh g_{NCA}^{-1}
[2] C_{rev}: reversible capacity obtained from delithiation step during formation cycle
[3] CV phases only during charge step for full cells and NCA half cells
[4] CV phases only for T-cells, not for coin cells

The termination criteria for the Si coin half cell, however, are different from those of the NCA half cell. During formation, the Si half cell was first lithiated until the nominal capacity of 6.636 mAh was reached and was then delithiated until a potential threshold of 1.0 V was reached. This capacity-based lithiation step is necessary because of the flat potential plateau during the initial amorphization process of crystalline Si (see Figure 1 in Ref. [5]). The total capacity of the delithiation step is the reversible capacity C_{rev} during cell formation. For the Si anode coin half cells, this value is 6.194 mAh. In order to not over-lithiate the cell during the subsequent stabilization cycles, this delithiation capacity is used as a termination criterion for the lithiation steps of the subsequent stabilization cycles instead of the nominal capacity. Graf et al. [6] showed that during these subsequent stabilization cycles (or cycling in general), Si can still undergo further amorphization if the half cell potential is below 170 mV. The amorphization process can be observed by a certain peak in the differential capacity curve, as can be seen in Figure 4 of Ref. [6]. According to the new capacity cut-off criterion, the C-Rates are adjusted to meet this reversible (delithiation) capacity instead of the nominal capacity. These lithiation and delithiation capacities can also be determined for the cathode half cell and the full cell setups. However, the exact values are of no further importance here, because both of these setups can be cycled using cut-off potentials for the charge and discharge step and no capacity-based steps are needed. The initial lithiation capacity is greater than the nominal capacity because the nominal capacity is based on the design parameter of 185 mAh g_{NCA}^{-1} on full cell level that should be reached after the formation and stabilization are completed. Note that, similarly to the Si anode, the NCA is not fully utilized and thus never reaches its theoretical gravimetric capacity of 279 mAh g^{-1} which would correspond to complete delithiation [7].

Open-Circuit Potential Measurement

After the formation and stabilization procedure was completed, the quasi open-circuit potential (qOCP) measurement was conducted for both, coin cells and T-cells. During the qOCP measurement, a C-Rate of $1/50\,C$ is applied to the cells. It is important to note that, for this test, the termination criterion of the lithiation step for the Si half cell was explicitly set to $0.170\,V$. Above this value, amorphization processes are not expected to occur [6]. Accordingly, no further amorphization of silicon is assumed. On another note, the qOCP measurement for the coin cells does not include a constant voltage (CV) phase, while the test for the T-cell does. The exact cycling procedure is given in Table S3, where the nomenclature for the "charge" and "discharge" steps is that of a full cell. Hence, the charge step is equal to a lithiation of the Si anode and a delithiation of the NCA cathode and vice versa for the discharge step.

In addition to the qOCP measurement using constant current (CC) phases only, as described above, a pulsed OCP (pulsed open-circuit potential (pOCP)) measurement was conducted. The pOCP measurement procedure is inspired by classical galvanostatic intermittent titration technique (GITT) measurements but no titration is carried out, while the quasi-OCP (qOCP) measurement consists of a plain CC (dis)charge. The pOCP test was conducted in the same climate chamber using the same potentiostat as during the previous tests and was performed for the coin cells only. The procedure is as follows: The cells were preconditioned via a CCCV discharge procedure ($1/50\,C$ CC, $1/200\,C$ CV cut-off), followed by a $2\,h$ open-circuit phase. From this discharged state, the pOCP procedure starts. The cells were charged using $1/50\,C$ CC steps until 5% state of charge (SoC) was charged. Each of these steps was followed by a $2\,h$ relaxation phase at open-circuit conditions. Upon reaching the upper voltage limit of $4.2\,V$, charging in 5% SoC steps continued via a CV phase. The charging process ended once the current during the CV phase dropped below a threshold of $1/200\,C$. After this, the cells relaxed at open-circuit conditions for $2\,h$ again. Subsequently, the cells were discharged using the same procedure as for the charge, i.e., $1/50\,C$ CC discharge using 5% SoC steps with a subsequent CV phase at $2.8\,V$ using 5% SoC steps, terminated when the current dropped below $1/200\,C$, always followed by $2\,h$ of open-circuit.

Both tests, qOCP and pOCP, were conducted with a higher C-Rate of $1/10\,C$ instead of $1/50\,C$ for the CC phases, too. The tests are compared to one another in order to investigate the qOCP as well as the polarization behavior at low currents.

Rate Test

Subsequent to the qOCP measurement, a rate test was conducted for the T-cells in order to validate the model using higher C-Rates of up to $10\,C$. The rate test procedure for each C-Rate is as follows: The cell is preconditioned to $2.8\,V$ using a $1/200\,C$ CV discharge phase. Then, the cell is charged using a CCCV phase, relaxes at open-circuit conditions for $45\,min$, is discharged using a CCCV phase, and relaxes at open-circuit conditions for $45\,min$ again. The C-Rate of the CC phases is varied for the charge and discharge steps ($1/10\,C$, $1/5\,C$, $1/3\,C$, $1/2\,C$, $1\,C$, $2\,C$, $3\,C$, $5\,C$, $10\,C$), while the CV cut-off current is fixed at $1/200\,C$. This way, the cell is preconditioned to a fully (dis)charged state before each (dis)charge step. For the evaluation, only the CC steps are taken into account.

S4. Supplementary Information on Electrode Kinetics

The anodic and cathodic charge transfer coefficients are assumed to be $\alpha_a = \alpha_c = 0.5$. However, this does not necessarily have to be the case, especially for materials with a pronounced qOCP hysteresis such as silicon. Chandrasekaran et al. [8], for example, utilized a simulation model for Si single particles to investigate the influence of asymmetric charge transfer coefficients that still hold $\alpha_a + \alpha_c = 1$. Sethuraman et al. [9] on the other hand fitted the apparent transfer coefficients to measurement data. Their fit resulted in apparent coefficients much greater than 0.5, and they interpret these results as complex lithiation and delithiation reactions [9]. They also state that the apparent coefficients can

be influenced by stress effects, particle size, and sample morphology. Because their thin films are morphologically largely different to the electrode in the present study, idealized values of $\alpha_a = \alpha_c = 0.5$ are used here. Just as for the solid-phase diffusion coefficient and the exchange current density, an in-depth experimental investigation regarding the sensitivity of the charge transfer coefficients with respect to the reaction direction, the degree of lithiation, and the temperature would be of great value. Depending on the experimental setup, the morphology, especially the active surface area or the particle size, might be of interest for such a study.

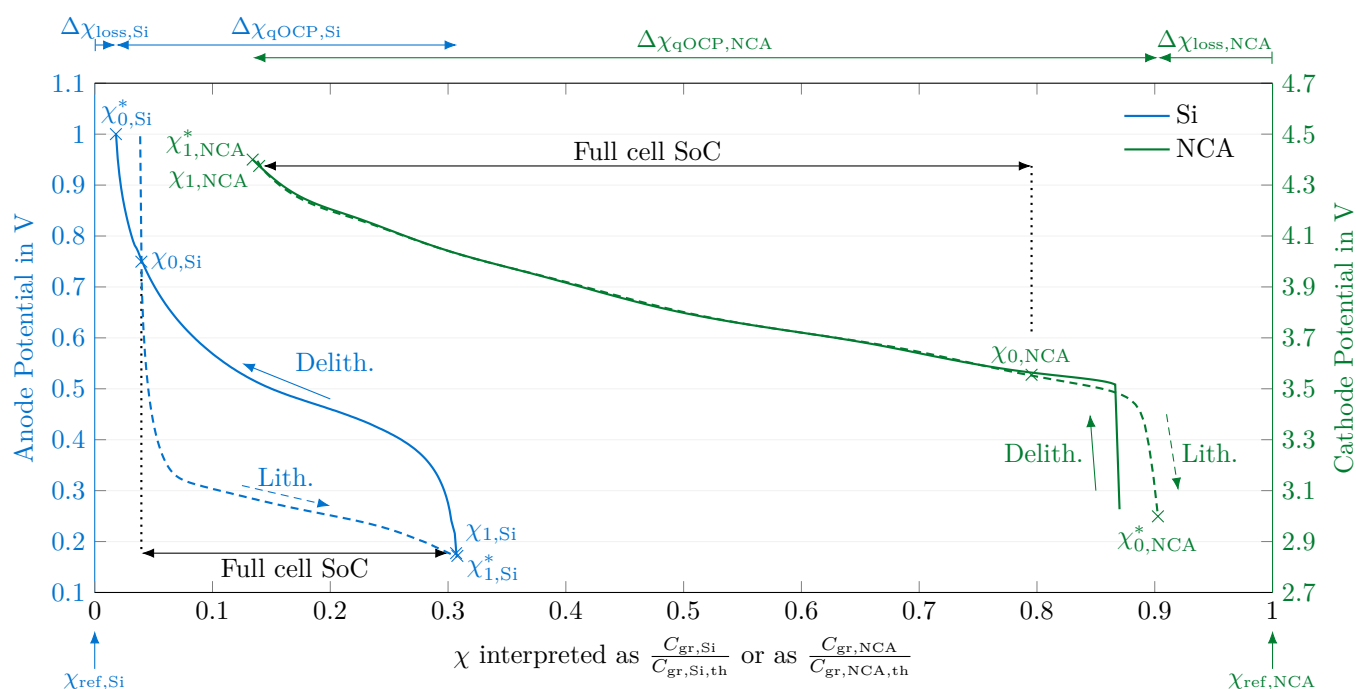### S5. Supplementary Information on the Transformation to the Degree of Lithiation

In a **first step**, material properties and sample values are defined. In a **second step**, the reference state χ_{ref} is defined, which represents the pristine state of the electrode. For the Si anode, a pristine degree of lithiation (DoL) of $\chi_{ref} = 0$ is assumed, as the electrode is not pre-lithiated. For the NCA cathode, a pristine DoL of $\chi_{ref} = 1$ is assumed. In a **third step** and starting from the reference state, the formation and stabilization losses give a rough estimate for the DoL on one end of the measured range. This state is not the reference state, because generally, the losses are non-zero, and it also is not equal to the state of the fully discharged full cell, because of the measured overhang of the half cells. Hence, this quantity is called χ_0^*, because it is close to but not equal to the DoL at SoC = 0%. In a **fourth step**, the last full cell discharge during the qOCP test is evaluated, which yields the utilization of the electrode. Starting from the state identified in the previous step, the utilization range gives a new state which is called χ_1^*, because it is close to but not equal to the DoL at SoC = 100%. In a **fifth step** and with knowledge of the half cell potentials at a full cell SoC of 0% and 100% from the electrode balancing process (Figures 2 and A1 in the main document), the DoL for these exact SoC values can be identified. This yields the DoL values χ_0 and χ_1 for the anode and cathode half cell for full cell charging and discharging (lines 1, 2, 4, and 5 of step 5 in Table S4). Finally, averaging the values of χ_0 (and χ_1) for a charge and discharge of each electrode individually gives a unified value for the respective electrode (lines 3 and 6 of step 5 in Table S4). This averaging results in a unified vector for the charge and discharge. Such a unified vector is important for the model when simulating full cycles (major loops) to capture the hysteresis effect. Without a unified vector, i.e., with different degrees of lithiation for the lithiation and delithiation curve at a given full cell SoC, switching between these curves due to a change in the sign of the cell current would introduce errors. The final results of the transformation to the DoL are shown in Figure S1.

Note that in Figure S1, the only exact values from Table S4 are χ_0 and χ_1. The values for $\Delta\chi_{loss}$, $\Delta\chi_{qOCP}$, and χ^* in the figure are not identical to those in the table, because the table shows intermediate results while the figure shows the results for the final x-axis transformation. However, every value in the figure is mapped true to scale to maintain traceablity.

Table S4. Step-by-step overview for the data conversion from the measured charge throughput of half cell setups to the degree of lithiation (DoL) of the individual electrode, and also of the alignment of the data with a corresponding full cell SoC of 0% and 100%. The reference state is set to be the fully delithiated/lithiated anode/cathode half cell. The starred versions χ^* correspond to the DoL of the measured half cell, while the unstarred versions χ correspond to the fully (dis)charged full cell. Index 1 stands for 100% full cell SoC and index 0 for 0%. **Step 1:** Material parameters and sample values. **Step 2:** Starting point assumption. **Step 3:** Evaluation of formation and stabilization losses. **Step 4:** Evaluation of qOCP data. **Step 5:** Identification of the electrode DoL for a full cell SoC of 0% and 100%. The values vary for the individual fittings for the full cell charge and discharge process and were averaged in order to obtain a unified DoL vector for each electrode.

			Si‖Li coin cell	NCA‖Li coin cell
Step 1	theoretical gravimetric capacity	$C_{\mathrm{gr,th}}$	$3579\,\mathrm{mAh\,g_{Si}^{-1}}$	$279\,\mathrm{mAh\,g_{NCA}^{-1}}$
	active material mass	m_{AM}	$5.53\,\mathrm{mg}$	$29.97\,\mathrm{mg}$
Step 2	DoL start (assumption)	χ_{ref}	0	1
Step 3	charge losses formation & stabilization	C_{loss}	$0.568\,\mathrm{mAh}$	$0.952\,\mathrm{mAh}$
		$C_{\mathrm{gr,loss}}$	$102.71\,\mathrm{mAh\,g_{Si}^{-1}}$	$31.77\,\mathrm{mAh\,g_{NCA}^{-1}}$
		$\Delta\chi_{\mathrm{loss}}$	0.0287	0.1139
	DoL at reference state	χ_0^*	0.0287	0.8861
Step 4	charge throughput during qOCP test	C_{qOCP}	$5.517\,\mathrm{mAh}$	$6.271\,\mathrm{mAh}$
		$C_{\mathrm{gr,qOCP}}$	$997.65\,\mathrm{mAh\,g_{Si}^{-1}}$	$209.24\,\mathrm{mAh\,g_{NCA}^{-1}}$
		$\Delta\chi_{\mathrm{qOCP}}$	0.2788	0.7500
	DoL at opposite reference state	χ_1^*	0.3075	0.1361
Step 5	half cell DoL at	discharge	0.0495	0.7808
	full cell SoC 0%	charge	0.0296	0.8100
		average χ_0	0.0396	0.7954
	half cell DoL at	discharge	0.3071	0.1376
	full cell SoC 100%	charge	0.3063	0.1417
		average χ_1	0.3068	0.1396

Figure S1. Quasi open-circuit potential of the measured Si and NCA half cell for the (de)lithiation as used in the model. The data are balanced to the full cell potential (see Figures 2 and A1 in the main document) and transformed to refer to the calculated degree of lithiation (DoL) χ of the respective electrode. The DoL is the capacity stored in the material relative to the fully lithiated state with $C_{gr,Si,th} = 3579\,\mathrm{mAh\,g^{-1}}$ and $C_{gr,NCA,th} = 279\,\mathrm{mAh\,g^{-1}}$. A schematic for the axis transformation from measured charge throughput to the DoL is shown via labeled arrows for ranges and crosses for discrete states.

References

1. Jantke, D.; Bernhard, R.; Hanelt, E.; Buhrmester, T.; Pfeiffer, J.; Haufe, S. Silicon-Dominant Anodes Based on Microscale Silicon Particles under Partial Lithiation with High Capacity and Cycle Stability. *Journal of The Electrochemical Society* **2019**, *166*, A3881–A3885. https://doi.org/10.1149/2.1311915jes.
2. Landesfeind, J.; Hattendorff, J.; Ehrl, A.; Wall, W.A.; Gasteiger, H.A. Tortuosity Determination of Battery Electrodes and Separators by Impedance Spectroscopy. *Journal of The Electrochemical Society* **2016**, *163*, A1372–A1387. https://doi.org/10.1149/2.1141607jes.
3. Habedank, J.B.; Kraft, L.; Rheinfeld, A.; Krezdorn, C.; Jossen, A.; Zaeh, M.F. Increasing the Discharge Rate Capability of Lithium-Ion Cells with Laser-Structured Graphite Anodes: Modeling and Simulation. *Journal of The Electrochemical Society* **2018**, *165*, A1563–A1573. https://doi.org/10.1149/2.1181807jes.
4. Wetjen, M.; Solchenbach, S.; Pritzl, D.; Hou, J.; Tileli, V.; Gasteiger, H.A. Morphological Changes of Silicon Nanoparticles and the Influence of Cutoff Potentials in Silicon-Graphite Electrodes. *Journal of The Electrochemical Society* **2018**, *165*, A1503–A1514. https://doi.org/10.1149/2.1261807jes.
5. Li, J.; Dahn, J.R. An In Situ X-Ray Diffraction Study of the Reaction of Li with Crystalline Si. *Journal of Power Sources* **2007**, *154*, A156. https://doi.org/10.1149/1.2409862.
6. Graf, M.; Berg, C.; Bernhard, R.; Haufe, S.; Pfeiffer, J.; Gasteiger, H.A. Effect and Progress of the Amorphization Process for Microscale Silicon Particles under Partial Lithiation as Active Material in Lithium-Ion Batteries. *Journal of The Electrochemical Society* **2022**, *169*, 020536. https://doi.org/10.1149/1945-7111/ac4b80.
7. Nitta, N.; Wu, F.; Lee, J.T.; Yushin, G. Li-ion battery materials: present and future. *Materials Today* **2015**, *18*, 252–264. https://doi.org/10.1016/j.mattod.2014.10.040.
8. Chandrasekaran, R.; Magasinski, A.; Yushin, G.; Fuller, T.F. Analysis of Lithium Insertion/Deinsertion in a Silicon Electrode Particle at Room Temperature. *Journal of Power Sources* **2010**, *157*, A1139. https://doi.org/10.1149/1.3474225.
9. Sethuraman, V.A.; Srinivasan, V.; Newman, J. Analysis of Electrochemical Lithiation and Delithiation Kinetics in Silicon. *Journal of The Electrochemical Society* **2013**, *160*, A394–A403. https://doi.org/10.1149/2.008303jes.